Stochastic inversion of seismic PP and PS data for reservoir parameter estimation

Jinsong Chen*, Lawrence Berkeley National Laboratory, and Michael E. Glinsky, ION Geophysical

Summary

We develop a hierarchical Bayesian model to invert seismic PP and converted-wave (i.e., PS) data for reservoir parameters. The model is an extension of the model-based Bayesian method by Gunning and Glinsky (2004) with converted wave responses and PS time registration as additional data and with two-way PS travel time and PS reflectivity as additional unknowns. We implement the model by revising their open-source software, 'Delivery', written in Java. We demonstrate the use of the revised codes by applying them to two synthetic cases. One is a three-layer sand wedge model with variable thickness, and the other is a six-layer floating-grain model based on actual field data. The case study results show that seismic PS data greatly enhances the resolution of seismic data for thin layers, and they provide more information on reservoir parameters than far-offset PP data.

Introduction

Multicomponent seismic surveying has been used for hydrocarbon exploration more than a decade because it can capture the seismic wave-field more completely than conventional single-element techniques (Stewart et al., 2002). Many types of energy conversion may occur when seismic waves pass through the underlying earth. However, transmitted or multiple conversions generally have much lower amplitudes than the P-down and S-up reflection (Rodriguez-Saurez, 2000). Consequently, for many applications of multi-component seismic data, the use of converted-wave or PS images receives much attention (Stewart et al., 2002; Mahmoudian and Margrave, 2004; Veire and Landro, 2006).

Several obstacles exist currently that make the use of converted-wave data, as a routine practice, difficult. The first one is the high acquisition cost of collecting multicomponent seismic data compared to conventional seismic surveys. The second one is that multicomponent data processing is still challenging. Compared with P-wave velocity analysis, identifying pure S-wave events in multicomponent seismic data is much harder (Veire and Landro, 2006). Finally, we still do not have good methods to jointly integrate multiple seismic data, especially in the sense of joint inversion, because PP and PS data are recorded in different time domains. This study is an effort to combine seismic PP and converted-wave for estimating reservoir parameters using a Bayesian hierarchical framework.

We extend the model-based Bayesian method developed by Gunning and Glinsky (2004) for inverting seismic AVO data, by revising their open-source Java codes (i.e., 'Delivery') to allow converted-wave responses and PS event time registration as additional data. We use the same rock physics models and Markov chain Monte Carlo (MCMC) sampling strategies as Delivery. Since this study is built on the previous work, the subsequent descriptions will be focused on the new development and applications, and the details of other parts can be found in Gunning and Glinsky (2004).

Method

Hierarchical Bayesian model

We use the same notations as Gunning and Glinsky (2004) and assume the subsurface can be divided into n horizontal layers. We consider reservoir parameters at each layer as unknowns, which include (1) porosity and net-to-gross (i.e., the ratio of permeable to impermeable rock by volume), (2) fluid saturation (e.g., brine, oil, and gas saturation), and (3) rock physics attributes of permeable and impermeable rocks (e.g., P-wave and S-wave velocity and density). For ease of description, we let vector $\boldsymbol{\alpha}$ represent all the parameters related to the rock physics model.

We consider effective seismic P-wave and S-wave velocity ($\mathbf{v}_p$ and $\mathbf{v}_s$) and density ($\boldsymbol{\rho}$), and seismic PP and PS reflectivity ($\mathbf{R}_{pp}$ and $\mathbf{R}_{ps}$) as unknowns. They are functions of rock physics parameters through suitable rock physics models. We consider PP traveltime ($\mathbf{t}_{pp}$) as a primary unknown, and both layer-thickness ($\mathbf{d}$) and PS traveltime ($\mathbf{t}_{ps}$) can be derived from the PP traveltime and associated effective seismic attributes. The data used for inversion include seismic PP and PS full-waveforms ($\mathbf{S}_{pp}$, and $\mathbf{S}_{ps}$) and PP and PS event registration time ($\mathbf{T}_{pp}$ and $\mathbf{T}_{ps}$). If available, they include other information from nearby boreholes, such as thickness constraints ($\mathbf{D}_b$).

Figure 1 shows all the unknowns, available data, and their relationships, and the dashed rectangle highlights our extension to Delivery. Specifically, we add two unknowns related to converted wave (i.e., $\mathbf{t}_{ps}$ and $\mathbf{R}_{ps}$) and two new data (i.e., $\mathbf{T}_{ps}$ and $\mathbf{S}_{ps}$). Following the direct graphical model, we have the following hierarchical Bayesian model:

$$f(\boldsymbol{\alpha}, \mathbf{t}_{pp}, \mathbf{t}_{ps}, \mathbf{d}, \mathbf{v}_p, \mathbf{v}_s, \boldsymbol{\rho}, \mathbf{R}_{pp}, \mathbf{R}_{ps} \mid \mathbf{S}_{pp}, \mathbf{S}_{ps}, \mathbf{T}_{pp}, \mathbf{T}_{ps}, \mathbf{D}_b)$$

$$\propto f(\mathbf{S}_{pp} \mid \mathbf{t}_{pp}, \mathbf{R}_{pp}) f(\mathbf{S}_{ps} \mid \mathbf{t}_{ps}, \mathbf{R}_{ps}) f(\mathbf{T}_{pp} \mid \mathbf{t}_{pp})$$

$$\times f(\mathbf{T}_{ps} \mid \mathbf{t}_{ps}) f(\mathbf{D}_b \mid \mathbf{d}) f(\mathbf{R}_{pp} \mid \mathbf{v}_p, \mathbf{v}_s, \boldsymbol{\rho}) \qquad (1)$$

$$\times f(\mathbf{R}_{ps} \mid \mathbf{v}_p, \mathbf{v}_s, \boldsymbol{\rho}) f(\mathbf{d} \mid \mathbf{t}_{pp}, \mathbf{v}_p) f(\mathbf{t}_{ps} \mid \mathbf{t}_{pp}, \mathbf{v}_p, \mathbf{v}_s)$$

$$\times f(\mathbf{v}_p, \mathbf{v}_s, \boldsymbol{\rho} \mid \boldsymbol{\alpha}) f(\boldsymbol{\alpha}) f(\mathbf{t}_{pp}).$$

Equation 1 defines a joint posterior probability distribution function of all unknown parameters, up to a normalizing constant. The first five terms on the right side of the equation are the likelihood functions of available data, which link data to unknowns, and all other terms on the right side are the prior probability distributions, derived from other sources of information. We define all the likelihood functions and prior distributions in a similar way to Delivery (see Gunning and Glinsky, 2004). In the following, we only describe the new development.

PP and PS reflectivities

We use the linearized Zoeppritz approximations (Aki and Richard, 1980) to obtain PP and PS reflectivity at an interface, which are given below:

$$R_{pp} = \frac{1}{2}\left(\frac{\Delta V_p}{V_p} + \frac{\Delta \rho}{\rho} \right)$$

$$+ \frac{1}{2}\left[\frac{\Delta V_p}{V_p} - 4\left(\frac{V_s}{V_p} \right)^2 \left(\frac{\Delta \rho}{\rho} + 2\frac{\Delta V_s}{V_s} \right) \right] \theta^2 + O(\theta^4), \qquad (2)$$

$$R_{ps} = -\frac{1}{2}\left[\frac{\Delta \rho}{\rho} + 2\left(\frac{V_s}{V_p} \right)\left(\frac{\Delta \rho}{\rho} + 2\frac{\Delta V_s}{V_s} \right) \right] \theta + O(\theta^3). \qquad (3)$$

In equations 2 and 3, $V_p = (V_{p1} + V_{p2})/2$, $V_s = (V_{s1} + V_{s2})/2$, $\rho = (\rho_1 + \rho_2)/2$, $\Delta V_p = V_{p2} - V_{p1}$, $\Delta V_s = V_{s2} - V_{s1}$, and $\Delta \rho = \rho_2 - \rho_1$, where ($V_{p1}$, V_{s1}, ρ_1) and (V_{p2}, V_{s2}, ρ_2) are P- and S-wave velocity and density in the layers above and below the interface. Symbol θ is the PP incident angle in the unit of radius. The PP and PS reflectivities have the fourth and third order of accuracy in terms of the incident angle.

Linkages between PP and PS data and event time registration

Traditional methods for joint inversion of PP and PS data are primarily based on mapping of PS data to PP time (or domain conversion), in which PS data are considered as additional seismic stacks. Although this approach is simple to implement, it suffers from difficulties, such as wavelet distortion (Bansal and Matheney, 2010), because the conversion of PS time to PP time needs interval seismic P-to-S velocity ratios, which are not known *a priori*.

In this study, we avoid the PP-to-PS domain conversion and use PS data directly in the PS time domain. We first pick one or more PS events from PS seismograms that have good correspondence with the PP seismograms along the same profile, and we refer them to as the master PS horizons. In the

forward simulation, we calculate all the PS times relative to the master horizons.

The use of event time registration as data is one of main advantages of Delivery as well as the current extension because PP event time is directly related to P-wave velocity and PS event time directly related to P-wave and S-wave velocity. They provide additional information to constrain the estimates of P-wave and S-wave velocity beyond the reflectivity based PP and PS full-waveforms.

Examples

We use two examples to test the revised codes and to demonstrate the benefits of including converted-wave data in reservoir parameter estimation. The first example is a three-layer wedge model with variable thickness, which is similar to the one by Gunning and Glinsky (2004) and Puryear and Castagna (2008). In the example, we will show how converted-wave data help to improve parameter estimation in thin layers. The second example is based on actual field data given by Gunning and Glinsky (2007) with six layers. We will show how converted-wave data help to estimate floating-grain fraction, which was demonstrated by Gunning and Glinsky (2007) to be a difficult parameter to estimate under the field conditions.

In both examples, we use the PP and PS wavelets typical of those derived from field borehole logs for sparse-spike inversion using the method of Gunning and Glinsky (2006). The PP and PS wavelets have the peak frequencies of 23 Hz and 13 Hz, respectively (see Figure 2).

Three-layer sand wedge model

We use the same three-layer sand wedge model given by Gunning and Glinsky (2004) to test the developed method. In this model, a sand wedge is pinched out by the surrounding shale layers. Based on the PP wavelet given in Figure 2 and using the formula from Chung and Lawton (1995), we get the PP tuning thickness of 28 m. For this study, we let the sand wedge thickness increase from 1/8 to 5/4 of the PP tuning thickness with an increment of 1/8 tuning thickness. This yields the thickness of 3.5, 7, 10.5, 14, 17.5, 21, 24.5, 28, 31.5, and 35 m. The true net-to-gross of the sand wedge is 0.5. For inversion, we set the prior as the truncated normal distribution with the true values as mean and 0.5 as the standard deviation. The rock physics model used for this study is given by Mavko et al. (1998, page 297) based on data from Han (1986) for tight-gas sandstones.

We generate synthetic PP and PS data by using equations 2 and 3 to calculate reflectivity. At the top interface of the sand wedge, the reflectivities of the near PP stack (incident angle = 6 degrees), the far PP stack (incident angle = 30 degrees), and the far PS stack (incident angle = 30 degrees) are 0.0864, 0.0677, and -0.1003, respectively. At its bottom interface, the reflectivities of PP near and far stacks and PS far stack are -0.0860, -0.0602, and 0.1179. We convolved those reflectivities with the given wavelets (see Figure 2) to get

seismic full waveforms. Figure 3 shows the synthetic seismic data, and we assume those data have Gaussian random noise with the standard deviation of 0.005.

Inversion results and analysis

We invert the synthetic data for ten different thicknesses using three different sets of data in the inversion. They are: (1) only near-offset PP stack, (2) the near and far PP stacks, and (3) the near PP stack and the far PS stack. Figure 4 shows the medians, 95% predictive intervals, and the true values for (a) the net-to-gross (NG), (b) thickness, (c) P-wave velocity, and (d) S-wave velocity as a function of wedge thickness. The black squares and the dashed lines in each figure show the true values and the prior bounds. The red, green, and blue lines are the estimates obtained using the only the near PP stack, the near and far PP stacks, and the near PP stack and the far PS stack. The solid lines represent the estimated medians and the dashed lines represent 95% predictive intervals.

Comparing the estimated NG, and the P-wave and S-wave velocities with their corresponding true values, we found that when using only the near PP stack data, the estimated medians are very close to their true values for thickness greater than 17.5 m (i.e., 62.5% of the tuning thickness) but the estimates have significant uncertainty. By adding the far PP stack data, the estimated medians have good agreements with the true values as long as the wedge thickness is greater than 10.5 m (i.e., 37.5% of the tuning thickness). By replacing the PP far stack with the PS far stack, the estimated medians are unbiased for thicknesses greater than 7 m or even less. PS data is better at estimating thicknesses and NG of thin layers.

From this example, we can see that the use of converted wave significantly improves the resolution of parameter estimation. The possible reasons may include (1) the PS data extending the frequency range of data, (2) the PS wavelet providing additional information, and (3) the PS event time registration providing additional information.

Six-layer floating-grain model

We use the example B in Gunning and Glinsky (2007) as the second test case. The example is based on actual field data and has six layers with the fourth and sixth layers being oil reservoirs. A general layer sequence is given by (1) marl, (2) silt-marl stringer complex, (3) shale, (4) upper pay sand, (5) shale, and (6) lower pay sand. As pointed out by Gunning and Glinsky (2007), this is a difficult case study as the oil reservoirs are capped by a complex draping structure including thick, acoustically hard marls and thin, soft, silty layers.

Again, we use two-offset stack seismic data (i.e., near and far), which have the incident angles of 0 and 30 degrees. Table 1 lists PP reflectivity coefficients of the near and far stacks and the PS reflectivity coefficients of the far stack for

each layer interface, calculated using equations 2 and 3. We can see that the near PP reflectivity coefficients at the first two interfaces dominate the reflections from the three deeper interfaces. Both PP and PS far stacks provide much larger reflectivity at those deeper interfaces, with the PS reflectivity being slightly better than the PP reflectivity.

Inversion results and analysis

We use the same PP and PS wavelets as for the first example and the floating-grain model developed by DeMartini and Glinsky (2006) and reformulated by Gunning and Glinsky (2007) for Delivery. Our primary focus is on the estimate of floating-grain fraction, and we want to see what we can gain by including converted-wave data in the estimation. Based on the field data, we set the true floating-grain fraction to 3.5% and the net-to-gross ratio to 65+/-10%. Other parameters are set to be the most plausible values at this site (see Gunning and Glinsky, 2007 for details). For inversion, we give a prior of truncated Gaussian distribution with mean of 2% and standard deviation of 3% for the floating-grain fraction. This distribution gives significant prior probability to the zero-float (i.e., the clean sand case).

Figure 5 compares the estimated posterior probability distributions of floating-grain fraction and effective S-wave velocity in the upper and lower pay layers (i.e., layers 4 and 6) under various situations with their corresponding prior probability distributions. The black curves are the prior probability distributions, and the red, green, and blue curves are the estimated probability densities obtained using only the near PP stack, the near and far PP stacks, and the near PP and far PS stacks, respectively. The comparison between the results using the near and far PP stacks is similar to those by Gunning and Glinsky (2007). We can see that the far PS stack significantly improves the estimate of effective S-wave velocity (see column 2) and provides more information than the far PP stack when estimating the floating-grain fraction (see column 1, blue curves vs. green curves).

Conclusions

The extended Bayesian model is effective when jointly inverting PP and PS data. PS data can provide complementary information to PP data and thus have the potential of significantly improving parameter estimation results.
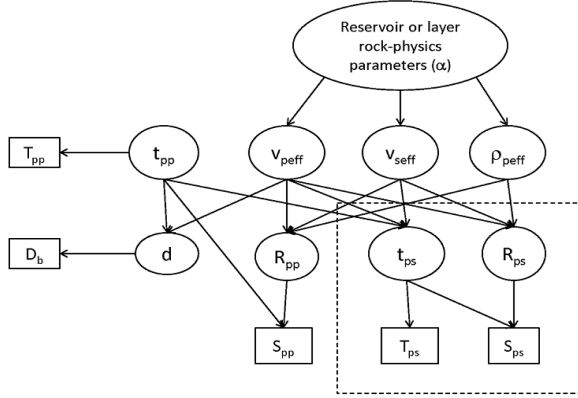
Acknowledgments

Figure 1. Hierarchical structure of unknown parameters and available data, where the arrows show conditional relationships.
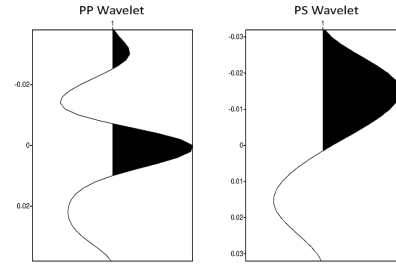

Figure 2. PP and PS wavelets, derived from borehole logs of a real field. They have the peak frequencies of 23 Hz and 13 Hz, respectively.
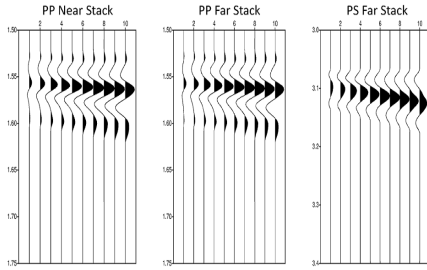

Figure 3. Seismic near PP stacks, far PP stacks, and far PS stacks for the three-layer wedge model. The PP data are in the PP time domain, while the PS data are in the PS time domain.
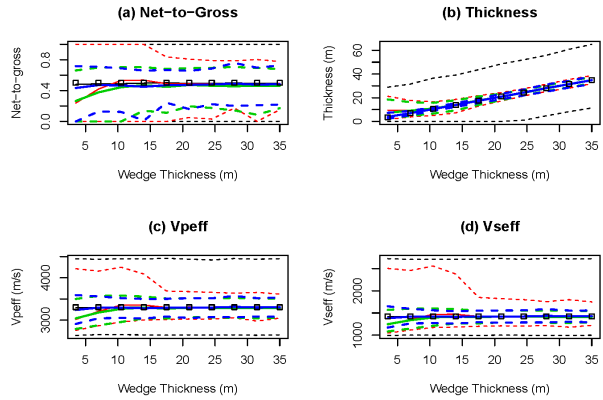

Figure 4. Comparison of prior and posterior estimates for the three-layer wedge model. The black shows the prior (dashes) and the true values (squares). The red, green, and blue show the medians (solid) and the 95% bounds (dashes) obtained from the near PP stacks, the near and far PP stacks, and the near PP and the far PS stacks.

Table 1: PP and PS reflectivity coefficients for the six-layer floating-grain model

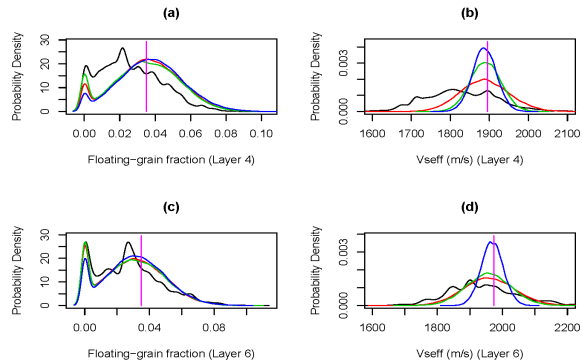| Interfaces	Near PP stack	Far PP stack	Far PS stack
Marl/stringer	-0.1586	-0.0887	0.2363
Stringer/shale	0.1007	0.0589	-0.1525
Shale/upper pay sand	0.0036	-0.0259	-0.0571
Upper pay sand/shale	0.0248	0.0394	0.0125
Shale/lower pay sand	-0.0100	-0.0352	-0.0386

Figure 5. Comparison between the prior and posterior estimates of floating-grain fraction ((a) and (c)) and S-wave velocity ((b) and (d)). The black curves and magenta vertical lines represent the prior and the true values. The red, green, and blue curves are the posterior probability densities obtained from the near PP stack, the near and far PP stacks, and the near PP and far PS stacks.

References

Bansal, R., and M. Mathency, 2010, Wavelet distortion correction due to domain conversion: Geophysics, 75, V77-V87.

Chung, H., and D. C. Lawton, 1995, Frequency characteristics of seismic reflections from thin beds: Canadian Journal of Exploration Geophysicists, 31, 32-37.

DeMartini, D. C., and M. E. Glinsky, 2006, A model for variation of velocity versus density trends in porous sedimentary rocks: Journal of Applied Physics, 100, 014910.

Gunning, J., and M. E. Glinsky, 2004, Delivery: an open-source model-based Bayesian seismic inversion program: Computers and Geosciences, 30.

Gunning, J., and M. E. Glinsky, 2007, Detection of reservoir quality using Bayesian seismic inversion: Geophysics, 72, R37-R49.

Mahmoudian, F., and G. F. Margrave, 2004, Three-parameter AVO inversion with PP and PS data using offset-binning: CREWES Report, 16.

Puryear, C. I., and J. P. Castagna, 2008, Layer-thickness determination and stratigraphic interpretation using spectral inversion: theory and application: Geophysics, 73, R37-R48.

Rodriguez-Saurez, C., 2000, Advanced marine methods: ocean- bottom and vertical cable analyses: PhD Thesis, University of Calgary.

Stewart, R. R., J. E. Gaiser, R. J. Brown, and D. C. Lawton, 2002, Converted-wave seismic exploration: methods: Geophysics, 67, 1348-1363.

Veire, H. H., and M. Landrø, 2006, Simultaneous inversion of PP and PS seismic data: Geophysics, 71, R1–R10